

Bag boundaries for quasispinor confinement within nanolanes on a graphene sheet

Yusef Koohsarian^{1,2,*} and Ali Naji^{1,†}

¹*School of Nano Science, Institute for Research in Fundamental Sciences (IPM), P.O. Box 19395-5531, Tehran, Iran*

²*School of Physics, Institute for Research in Fundamental Sciences (IPM), P.O. Box 19395-5531, Tehran, Iran*

We revisit the problem of bag boundary conditions within a field-theoretic approach to study confinement of massless Dirac quasispinors in monolayer graphene. While no-flux bag boundaries have previously been used to model lattice termination sites in graphene nanoribbons, we consider a generalized setting in which the confining boundaries are envisaged as arbitrary straight lines drawn across a graphene sheet and the quasispinor currents are allowed to partially permeate (leak) through such boundaries. We specifically focus on rectangular nanolanes defined as areas confined between a pair of parallel lines at arbitrary separation on an unbounded lattice. We show that such nanolanes exhibit a remarkable range of bandgap tunability depending on their boundary permeability and armchair, zigzag or intermediate orientation. We identify metalizable states whose bandgaps can continuously be decreased to zero by tuning boundary permeabilities, and insulating states whose bandgaps can be made significantly larger than those of graphene nanoribbons. The case of nanoribbons follows as a special limit from the nanolane model. In this case, we clarify certain inconsistencies in previous implementations of no-flux bag boundaries and show that the continuum approach reproduces the tight-binding bandgaps accurately (within just a few percent in relative deviation) even as the nanoribbon width is decreased to just a couple of lattice spacings.

I. INTRODUCTION

The discovery of graphene—the prominent single-layer honeycomb lattice of carbon atoms^{1–4}—has made a significant impact on a wide range of modern technological applications^{5–9}. The advances are made possible thanks to many remarkable transport, optical and mechanical properties that have since been uncovered for graphene and its derivatives. One of the key physical aspects of monolayer graphene is its gapless spectra of low-energy (electron-hole) excitations that emerge as massless Dirac quasispinors^{10–15}. This brings the low-energy physics of graphene into close analogy with the quantum field theory of Dirac spinors. Massless Dirac quasispinors are responsible for some of the most exotic phenomena observed in graphene such as anomalous quantum Hall effect^{16–18} and Klein tunneling^{19–21}. These have driven a substantial interest in field-theoretic formulations of graphene physics in the recent past^{11,22–25}.

While unbounded graphene has thoroughly been studied using field-theoretic methods, its other realizations such as graphene nanoribbons and carbon nanotubes have received less attention from that perspective^{26–31}. Graphene nanoribbons have emerged as promising semiconducting materials with tunable energy bandgap in room-temperature nanoelectronic applications^{32–34}. The most commonly studied cases of nanoribbons involve a regular, armchair or zigzag, arrangement of carbon atoms on their side edges. The bandgap of fixed-width nanoribbons can be calculated using standard tight-binding methods and is found to depend on the nanoribbon width and edge configuration^{35–38}. The presence of side edges raises the subtle issue of boundary conditions when a field-theoretic formulation is attempted. In the tight-binding approach, the boundaries are modeled by imposing Dirichlet-type boundary conditions on electronic wavefunctions at nanoribbon side edges³⁸. In the field-

theoretic approach, Dirichlet-type boundary conditions are useless due to their well-known inconsistency with Dirac equations. Instead, bag boundary conditions have recently been utilized to model vanishing quasispinor currents at lattice termination sites^{29–31}.

Bag models were originally proposed in quantum chromodynamics as a consistent route to confine Dirac spinors (quarks in hadrons) by imposing no-flux conditions along surface normals of an assumed confining volume (resembling an impermeable ‘bag’)^{42–49}. For armchair graphene nanoribbons^{26,27}, the consistency issue was addressed also via a particular type of boundary condition that admixed the so-called valleys of the energy band at armchair side edges. It was later shown³¹ that the proposed boundary condition is equivalent to the no-flux bag model even as sizable differences in predicted bandgaps persisted relative to tight-binding results²⁶.

In this paper, we revisit the problem of bag boundaries for quasispinor confinement in graphene by placing it in a broader context beyond its prior application to nanoribbons. Rather than considering them as lattice termination sites as done for nanoribbon, we envisage the boundaries as arbitrary in-plane lines that may be drawn across an unbounded graphene sheet. The specific case of interest in this work will be a pair of parallel straight lines which laterally confine a quasi-one-dimensional area of the sheet which we shall refer to as a *nanolane* (thus, also in contrast to nanoribbons, the width of such nanolanes can be treated as a continuous variable). The boundary orientation can be varied to define armchair, zigzag and intermediate nanolanes. Taking advantage of the continuum field-theoretic description, we introduce a generalized form of bag boundaries by allowing finite fluxes of quasispinors to permeate or ‘leak’ through the boundary lines. Thanks to its tractable analytical framework, the proposed model can be used to make a host of remarkable predictions. These include ‘metalizable’ arm-

chair and zigzag nanolanes whose bandgaps, unlike their nanoribbon counterparts, can be tuned *continuously* and reduced to zero by adjusting the difference in the permeabilities of the two boundaries. The predictions also include insulating armchair and zigzag nanolanes with large bandgaps exceeding those of typical nanoribbons.

Since the formulation of the current model is rather generic, its predictions could be relevant to a host of real situations involving imperfect (‘leaky’) electronic confinement in graphene. The boundary lines can be viewed as arrangements of adatoms or, when a graphene sheet is suspended over a rectangular trench, they can be viewed as the parallel lines of contact between the sheet and the edges of the trench. In the latter case, the contact lines may not necessarily be commensurate with armchair/zigzag edges of a nanoribbon and/or they may not necessarily be impermeable to quasipinor currents as in nanoribbons. These make the proposed nanolanes a more suitable modeling alternative in such cases.

The quantitative viability of our model is supported by comparing its predictions in the special limit of nanoribbons (Appendix A) with the tight-binding results^{35–38}. In contrast to Ref.²⁶, where nanoribbon bandgaps are studied through no-flux bag boundaries and sizable deviations from the tight-binding bandgaps at small widths are reported, our model reproduces the tight-binding results within relative differences of just a few percent even as the width is decreased down to a couple of lattice spacings. This signifies the extended applicability of the continuum field-theoretic approach in the present context.

In Section II, we provide a brief background on quasipinor formulation and discuss our predictions for armchair, zigzag and intermediate nanolanes in Sections III A–III C, respectively, with a conclusion in Section IV.

II. MODEL DESCRIPTION

A. Preliminaries on Dirac quasispinors in graphene

Quasipinor representation of electronic states in an unbounded monolayer graphene follows standardly from a tight-binding formulation of in-plane π -electron hopping between nearest-neighbor carbon atoms. Thanks to its two-dimensional (2D) honeycomb lattice, incorporating two triangular sublattices, an undoped monolayer displays conduction and valence energy bands in the 2D reciprocal (\mathbf{k}) space that meet at six individual Dirac points at the corners of the first Brillouin zone. Only two of the Dirac points turn out to be independent and can suitably be chosen as $\mathbf{K}_{\pm} = (0, \pm \frac{4\pi}{3d})$ where $d \simeq 2.46 \text{ \AA}$ is the lattice spacing. The low-energy excitations with wavevector $\mathbf{q} = \mathbf{k} - \mathbf{K}_{\pm}$, measured from the Dirac points, are found to obey independent massless Dirac equations, with identical linear energy dispersions $\epsilon_{\mathbf{q}} = \lambda \hbar \omega_{\mathbf{q}}$ where $\omega_{\mathbf{q}} = v_F |\mathbf{q}|$ and $v_F \simeq 10^6 \text{ m/s}$ is the Fermi velocity. While the subscripts \pm are used to denote the valley index associated with \mathbf{K}_{\pm} , the dispersion relation itself adopts positive

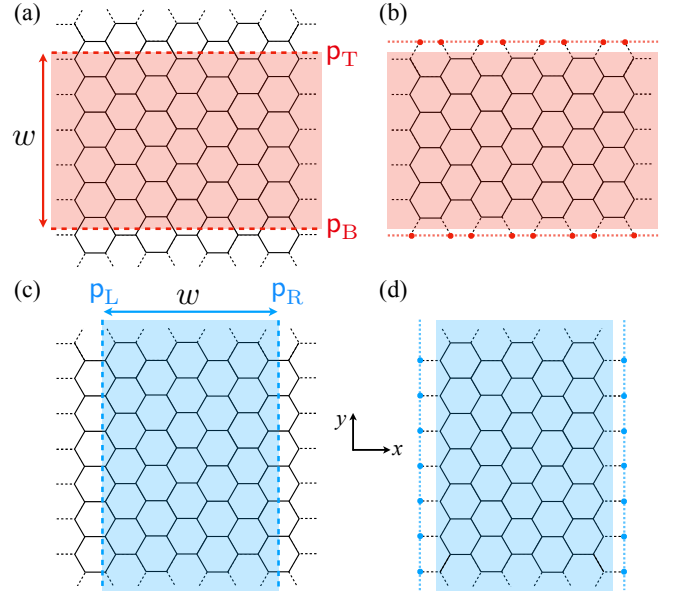


FIG. 1. Armchair (a) and zigzag (c) nanolanes (colored areas) are defined through boundaries (dashed lines) that can generally be permeable to quasipinor currents. They are characterized by permeability coefficients $p_{B,T}$ for the top/bottom and $p_{L,R}$ for the left/right boundaries, respectively. Armchair (b) and zigzag (d) nanoribbons are recovered as special limits of nanolanes upon shifting the boundaries (dotted lines) by a total offset of d to define lattice termination sites and setting the permeabilities equal to zero ($p_{B,T} = p_{L,R} = 0$).

and negative solutions identified by the (conduction versus valence) band index $\lambda = \pm 1$ which is intrinsically related to the sublattice (or quasipin) index, not being explicitly shown here. At each Dirac point, the probability amplitudes of Bloch wavefunction on the two underlying sublattices can be combined into the 2-spinor fields $\psi_{\pm, \mathbf{q}}(\mathbf{r})$, which themselves combine into a 4-spinor $\Psi_{\mathbf{q}}(\mathbf{r}) = (\psi_{+, \mathbf{q}}(\mathbf{r}), \psi_{-, \mathbf{q}}(\mathbf{r}))^T$, fulfilling

$$i v_F \gamma^0 \gamma^a \partial_a \Psi_{\mathbf{q}}(\mathbf{r}) = \omega_{\mathbf{q}} \Psi_{\mathbf{q}}(\mathbf{r}); \quad a = 1, 2, \quad (1)$$

where γ^a are defined using Pauli matrices as^{24,25}

$$\gamma^0 = \begin{pmatrix} \sigma_3 & 0 \\ 0 & \sigma_3 \end{pmatrix}, \gamma^1 = \begin{pmatrix} i\sigma_1 & 0 \\ 0 & i\sigma_1 \end{pmatrix}, \gamma^2 = \begin{pmatrix} i\sigma_2 & 0 \\ 0 & -i\sigma_2 \end{pmatrix}. \quad (2)$$

For brevity, we henceforth drop the subscript \mathbf{q} . The quasipinor currents $J^\nu = \Psi^\dagger \gamma^0 \gamma^\nu \Psi$ ($\nu = 0, 1, 2$) involve the spatial parts $J^a = J^a_+ + J^a_-$, with $J^\pm_a = \psi^\dagger_{\pm} i \sigma_3 \sigma_a \psi_{\pm}$ each incorporating electron/hole contributions.

B. Permeable bag boundaries

In principle, any external source that could break the isotropy of the π -electron distribution in monolayer graphene would produce an in-plane boundary condition on quasipinors. The schematic views of armchair and

zigzag nanolanes, envisaged in our study as rectangular areas of an unbounded graphene sheet, are depicted in Figs. 1a and c. For an armchair (zigzag) nanolane of width w , we choose the boundary positions as $y = \mp w/2$ ($x = \mp w/2$). The permeabilities of a given boundary to quasipinor currents associated with ψ_{\pm} are denoted by \mathbf{p}_{\pm} . The generalized (permeable) bag boundary conditions at a given boundary line thus reads

$$J_{\pm}^{\perp} \equiv \mathbf{J}_{\pm} \cdot \hat{\mathbf{n}} = \mathbf{p}_{\pm}, \quad (3)$$

where $\mathbf{J}_{\pm} = (J_{\pm}^1, J_{\pm}^2)$ and $\hat{\mathbf{n}} = (n_1, n_2)$ is the inward unit boundary normal. For simplicity, we drop the subscripts \pm given that, due to the time-reversal symmetry, the following calculations can similarly be repeated for either of the fields ψ_{\pm} . Hence, as shown in Figs. 1a and c, we proceed by denoting the permeability coefficients by $\mathbf{p}_{B,T}$ ($\mathbf{p}_{L,R}$) at the top/bottom (left/right) boundaries of armchair (zigzag) nanolanes, respectively. In general, the permeabilities can be functions of the wavevector. For the geometries at hand, we assume that they can be approximated by constants near the Dirac points.

Figures 1b and d show how armchair/zigzag nanoribbons can be recovered as special limits of nanolanes. For a nanolane width w , this involves setting the boundary permeabilities $\mathbf{p}_{B,T} = \mathbf{p}_{L,R} = 0$ and shifting the boundary lines by a total offset of d to the relevant lattice termination sites. As noted before, w can be varied continuously in the case of nanolanes but, evidently, it can only take a discrete set of values in nanoribbons. The limit of nanoribbons is discussed in Appendix A.

III. RESULTS

A. Armchair nanolanes

For an armchair nanolane, Eq. (1) can be solved inside the nanolane region ($|y| < w/2$, see Fig. 1a) as

$$\psi \propto e^{iq_{\parallel}x} [\alpha e^{iq_{\perp}y} + \beta e^{-iq_{\perp}y}], \quad (4)$$

where α and β are constant 2-spinors and $q_{\parallel,\perp}$ are longitudinal/transverse components of \mathbf{q} . Equation (3) can be written at the bottom (B) and top (T) boundaries as

$$\psi^{\dagger} \sigma_1 \psi|_{y=-w/2} = \mathbf{p}_B, \quad \psi^{\dagger} \sigma_1 \psi|_{y=w/2} = \mathbf{p}_T, \quad (5)$$

where we have used $\sigma_3 \sigma_2 = -i \sigma_1$. Equation (5) implies $(\alpha^{\dagger} \sigma_1 \beta + \beta^{\dagger} \sigma_1 \alpha) \sin(q_{\perp} w) = \mathbf{p}_T - \mathbf{p}_B$, or

$$\sin(q_{\perp} w) = \Delta, \quad (6)$$

where we have defined the *permeability mismatch* $\Delta \equiv \rho_T - \rho_B$ via normalized coefficients $\rho_{B,T} \equiv \mathbf{p}_{B,T} / (\alpha^{\dagger} \sigma_1 \beta + \beta^{\dagger} \sigma_1 \alpha)$. Note that $0 \leq \rho_{B,T} \leq 1$ give the permeation probability amplitudes at the boundaries and $0 \leq |\Delta| \leq 1$ covers all realizable cases in the present context.

The permissible values of $q_{\perp,n}$ follow from Eq. (6) and are standardly indexed by integer n . For the original

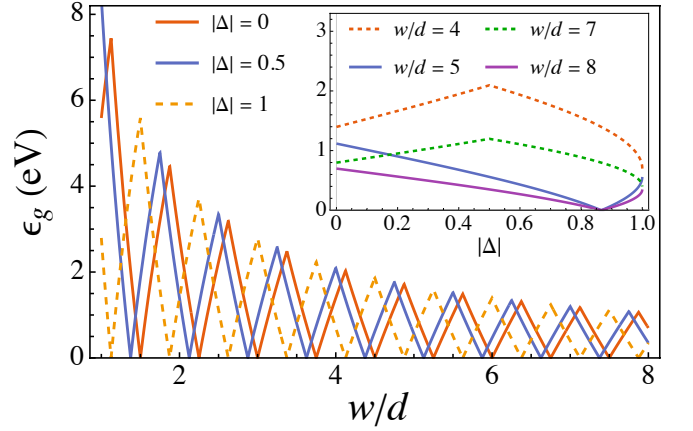


FIG. 2. Energy bandgap, ϵ_g , of armchair nanolanes is shown as a function of rescaled nanolane width, w/d , at fixed values of $|\Delta|$ as indicated on the graph. Inset shows ϵ_g as a function of $|\Delta|$ at fixed values of w/d .

wavevectors $\mathbf{k} = (k_{\parallel}, k_{\perp})$ in the first Brillouin zone, one finds $k_{\parallel} = q_{\parallel}$, which varies over the real axis, $k_{\perp,n} = 4\pi/(3d) + q_{\perp,n}$, which takes the discrete set of values

$$k_{\perp,n} = \frac{\pi}{w} \left[n + \frac{4}{3} \left(\frac{w}{d} \right) + \frac{1}{\pi} \sin^{-1} |\Delta| \right]. \quad (7)$$

The low-energy spectra of an armchair nanolane then follows as $E_n(k_{\parallel}) = \pm \hbar v_F \sqrt{k_{\parallel}^2 + k_{\perp,n}^2}$, giving the bandgap

$$\frac{\epsilon_g}{\hbar v_F} = \frac{2\pi}{w} \cdot \begin{cases} |\Lambda - \ell| & : 0 \leq \Lambda - \ell < \frac{1}{2}, \\ |\Lambda - \ell - 1| & : \frac{1}{2} \leq \Lambda - \ell < 1, \end{cases} \quad (8)$$

for nonnegative integer $\ell = 0, 1, 2, \dots$, and Λ defined as

$$\Lambda \equiv \frac{4}{3} \left(\frac{w}{d} \right) + \frac{1}{\pi} \sin^{-1} |\Delta|. \quad (9)$$

The gap function ϵ_g is shown in Fig. 2, main set, as a function of the nanolane width w for selected fixed values of $|\Delta|$. As dictated by Eq. (8), ϵ_g is a continuous piecewise linear function of w with specific peaks and troughs. The peak values of ϵ_g vary over a wide range (dropping from $\epsilon_g \sim 10$ eV to sub-eV values) as the nanolane width is increased modestly (from $w/d \sim 1$ up to 8).

The bandgap vanishes at the troughs. These particular widths thus identify the metallic states of armchair nanolanes. As seen in the graph, the peaks and troughs shift to the left as $|\Delta|$ is increased from zero. For a given w , this means that ϵ_g can vary nonmonotonically with $|\Delta|$. This raises another interesting question whether an armchair nanolane of a given width can be ‘metalized’; i.e., its gap can be reduced to zero by tuning $|\Delta|$.

To address this question, we show ϵ_g as a function of $|\Delta|$ for selected fixed values of w in the inset of Fig. 2. As seen, for $w/d = 4$ and 7 (dashed curves), the bandgap displays a cusp at $|\Delta| = 0.5$. By contrast, for $w/d = 5$ and 8 (solid curves), it displays a trough (resembling an

inverted cusp) that touches the $\epsilon_g = 0$ axis. These latter cases represent *metalizable* states of armchair nanolanes. For a nanolane of width w , these states are obtained when $1/2 \leq (4w/3d) - \ell < 1$ for nonnegative integer ℓ as noted above. Thus, an insulating nanolane even with sizable bandgap can be metalized by adjusting $|\Delta|$ to an appropriate value; e.g., for $w/d = 5$ and 8, this occurs at $|\Delta| \simeq 0.85$ (Fig. 2, inset).

Our results also reveal bandgap *universality* for $\Delta = 0$. This corresponds to symmetric armchair nanolanes with identical boundary conditions $\mathbf{p}_B = \mathbf{p}_T = \mathbf{p}$. In this case, the predicted bandgap (7) and, in fact, the whole spectrum of low-energy excitations become independent of the boundary permeability \mathbf{p} . This implies universal properties relative to quasispinor currents at the two boundaries which is itself indicative of coexisting time-reversal and parity-mirror symmetries in this special case. The time-reversal symmetry of the underlying graphene Dirac model guarantees block-diagonal Hamiltonian and γ -matrices (2). It thus allows one to impose the bag boundary conditions independently on the 2-spinor field ψ_{\pm} . On the other hand, since the quasispinor currents transform as $J_{\pm}^{\perp}(y) \rightarrow J_{\pm}^{\perp}(-y)$ under the mirror transformation $y \rightarrow -y$, this symmetry is preserved only if the two boundaries are identical. In asymmetric nanolanes with $\mathbf{p}_B \neq \mathbf{p}_T$, the mirror symmetry is violated locally which can be interpreted as unequal quasiparticle densities being induced near the boundaries.

B. Zigzag nanolanes

For a zigzag nanolane, Eq. (3) at the left (L) and right (R) boundaries (Fig. 1c) can be written as

$$-\psi^{\dagger} \sigma_2 \psi|_{x=-w/2} = \mathbf{p}_L, \quad -\psi^{\dagger} \sigma_2 \psi|_{x=w/2} = \mathbf{p}_R. \quad (10)$$

The solution for q_{\perp} , which here stands for the x -component of \mathbf{q} , follows from an equation similar to Eq. (6). In this case, we have $k_{\perp} = q_{\perp}$, or

$$k_{\perp,n} = \frac{\pi}{w} \left[n + \frac{1}{\pi} \sin^{-1} |\Delta| \right], \quad (11)$$

where Δ is analogously defined as $\Delta \equiv \rho_R - \rho_L$. We thus find the energy bandgap as

$$\frac{\epsilon_g}{\hbar v_F} = \frac{2}{w} \sin^{-1} |\Delta|. \quad (12)$$

The bandgap expression (12) is shown in the main set of Fig. 3 as a function of the width w/d at selected fixed values of $|\Delta|$ and in the inset of the figure as a function of $|\Delta|$ at selected fixed values of w/d . For $|\Delta| = 0$ and 1, these curves pass through the peaks and troughs of the corresponding curves in Fig. 2. As seen from Fig. 3, symmetric zigzag nanolanes with identical boundaries ($|\Delta| = 0$) are always metallic regardless of their width. The asymmetric zigzag nanolanes ($|\Delta| \neq 0$), on the other hand, are always insulating at finite width but, unlike

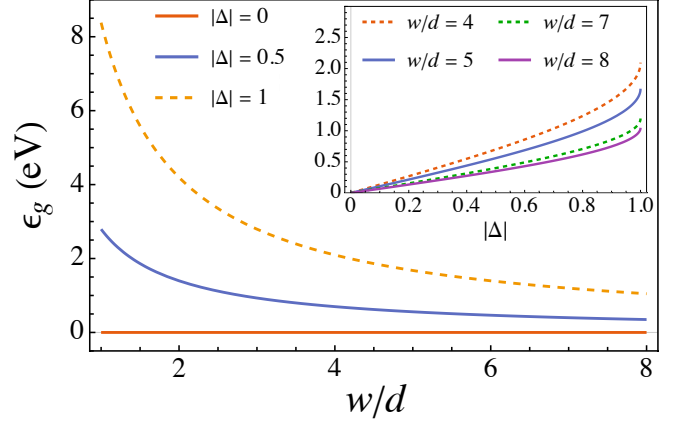


FIG. 3. Same as Fig. 2 but plotted here for zigzag nanolanes.

armchair nanolanes, all zigzag states can be metalized by tuning the permeability mismatch Δ . Also, in contrast to the latter case, the bandgap here monotonically increases with $|\Delta|$ (compare insets of Fig. 2 and 3).

C. Intermediate nanolanes

We now consider the intermediate case of a nanolane which is realized by rotating the honeycomb lattice by angle of α ; see Fig. 4a. In the aforementioned example of a suspended graphene sheet over a rectangular trench, this realization can be viewed as the lattice being rotated relative to the edges of the trench and the edges themselves being represented by the straight boundary lines of permeabilities \mathbf{p}_L and \mathbf{p}_R . It is clear that the nanolane bandgap will periodically change with α in such a way that for $\alpha = 2j\pi/6$ and $\alpha = (2j+1)\pi/6$, with nonnegative integer j , correspond to zigzag and armchair states, respectively. Using skew coordinates, it is straightforward to obtain the generalized form of the wavevector $k_{\perp,n}$ as

$$k_{\perp,n} = \frac{\pi}{w} \left[n + \frac{8}{3} \left(\frac{w}{d} \right) \sin \left(\frac{\pi}{6} - \alpha \right) + \frac{1}{\pi} \sin^{-1} |\Delta| \right]. \quad (13)$$

where $0 \leq \alpha \leq \pi/6$ and, for $\alpha = 0$ and $\pi/6$, the zigzag and armchair relations (11) and (7) are recovered, respectively. The bandgap of intermediate nanolane is given by Eq. (8) by replacing Λ in Eq. (9) with

$$\Lambda \rightarrow \frac{8}{3} \left(\frac{w}{d} \right) \sin \left(\frac{\pi}{6} - \alpha \right) + \frac{1}{\pi} \sin^{-1} |\Delta|. \quad (14)$$

The energy bandgap, ϵ_g , of an intermediate nanolane is plotted in Fig. 4b as a function of Δ and α for $w = 4d \simeq 1$ nm. As seen, ϵ_g along the α -axis has a generally armchair-like behavior, with a maximum gap of $\simeq 2$ eV.

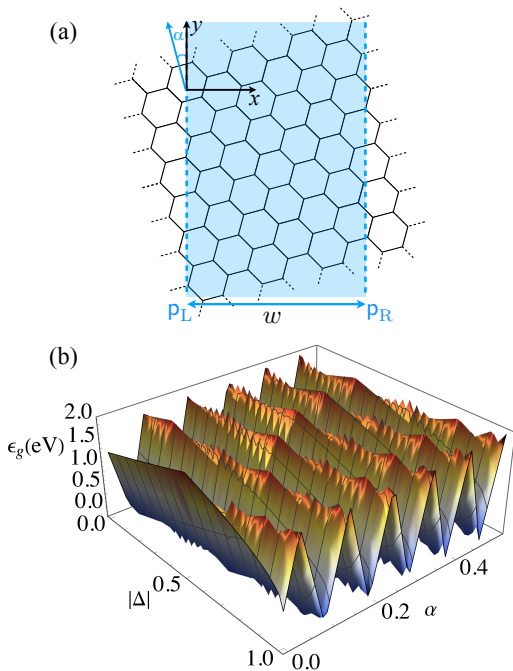


FIG. 4. (a) Schematic view for an intermediate realization of nanolane in which the honeycomb lattice is rotated by an angle of α (compare with Fig. 1c). (b) Energy bandgap, ϵ_g , for an intermediate nanolane of width $w = 4d$ is shown as a function of $|\Delta|$ and α varying over the range $0 \leq \alpha \leq \pi/6$.

IV. SUMMARY AND DISCUSSION

We have proposed a generalized form of bag boundary conditions to address confinement of massless Dirac quasipins within quasi-one-dimensional areas, defined as nanolanes, over a monolayer graphene sheet. The problem is formulated within a continuum field-theoretic approach that captures the essential physics of low-energy electronic excitations over the honeycomb lattice^{22–25}. The model nanolanes are constructed by (1) taking the nanolane boundaries as any pair of parallel straight lines at arbitrary distance from one another over an unbounded lattice, and (2) assigning finite permeabilities to quasipinor currents at the boundaries through an extension of standard no-flux bag boundary conditions. These constructions not only preserve formal consistency of the model with the underlying Dirac equation but they also allow for the nanolane properties (here, specifically, their bandgap) to be tuned via continuous variables. The latter include the nanolane width w and the mismatch $|\Delta|$ between permeability coefficients at the boundary lines.

Our analysis indeed reveals highly tunable bandgaps for nanolanes in armchair, zigzag and intermediate orientations. Armchair nanolanes exhibit both metalized and insulating states depending on w and $|\Delta|$. For a fixed w , the armchair bandgap varies nonmonotonically with $|\Delta|$. For widths in the range $1/2 \leq (4w/3d) - \ell < 1$ (with nonnegative integer ℓ), the bandgap can continuously be reduced to zero by varying $|\Delta|$. The latter

represent metalizable states of armchair nanolanes. By contrast, the zigzag bandgap varies monotonically with $|\Delta|$ and all zigzag states are metalizable regardless of their width. Insulating zigzag nanolanes thus present the more versatile case of continuous bandgap tunability. For symmetric nanolanes ($|\Delta| = 0$), the armchair bandgap is found to be universal (independent of $|\Delta|$), while the zigzag bandgap vanishes identically at all widths.

The quantitative predictions of our model remain accessible to experimental verification. Specifically, our results give predict sizable bandgaps, e.g., up to $\simeq 2$ eV for a nanometer-wide nanolane, larger than those obtained from Dirichlet tight-binding calculations in the case of nanoribbons^{35–38}. Our study should also facilitate theoretical modeling in a wider range of realistic situations involving nonideal (permeable) electronic confinement in graphene. Possible realizations of the modeled boundary lines may include arrays of adatoms deposited over a graphene sheet or, for a graphene sheet suspended over a rectangular trench, the parallel contact lines created between the sheet and the edges of the trench. While the proposed model can be viewed as a promising setting to study electronic control in graphene-based nanosystems^{5–9}, it is also important to analyze its predictions using other more comprehensive techniques such as first-principle calculations^{39–41} which, for nanoribbons, predict sizable corrections to the tight-binding results in closer agreement with experiments^{50–54}.

In the special limit of nanoribbons (impermeable nanolanes with widths varying only over a discrete set of admissible values), our approach reproduces the tight-binding bandgaps^{35–38} to within relative deviations of only a few percents even at small nanoribbon widths of a couple lattice spacings. (The bandgap calculation in our approach follows more straightforwardly in only a few steps as compared with the tight-binding approach³⁸.) In this limiting case, we clarify the source of discrepancies between the previous implementation of no-flux bag boundaries²⁶ and the tight-binding results (Appendix A).

Finally, we note that the special case of no-flux bag boundaries can also be implemented in its indirect form^{29,30} as $i\gamma^a n_a \psi = \psi$ while we have used its direct form (3). Our inspections indicate that the two formulations may not be necessarily equivalent and it is the latter that accurately reproduces the tight-binding results (in fact, the relevant nanoribbon subtypes $w/d = 3\ell \pm 1, 3\ell$ do not emerge in the former case^{29,30}). In the nanolane context, the distinction between the two formulations of bag boundaries is even more apparent, as the boundaries exhibit finite permeabilities to quasipinor currents.

Appendix A: Nanoribbons as no-flux nanolanes

To specialize our model to nanoribbons, we use no-flux bag boundaries $\mathbf{p}_{B,T} = 0$ ^{26–31} and displace the boundary lines with a total offset of d to coincide with the respective armchair and zigzag lattice termination sites

of nanoribbons³⁸ (see also Figs. 1b and d). Hence, for the limiting case of armchair nanoribbons, we find the modified form of Eq. (6) as

$$\sin[(k_{\perp} - 4\pi/3d)(w + d)] = 0. \quad (\text{A1})$$

In contrast to nanolanes, armchair nanoribbon width varies only over a discrete subset of values (subtypes) $w/d = 3\ell \pm 1$ and 3ℓ ^{35–38}. For $w/d = 3\ell - 1$, Eq. (A1) yields $k_{\perp,n} = n\pi/(w + d)$ reproducing the standard gapless energy band. For $w/d = 3\ell$ and $3\ell + 1$, Eq. (A1) yields $k_{\perp,n} = n\pi/(w + d) + 4\pi/(3d)$ and an energy band with no gapless states. In the implementation of bag boundaries for Dirac quasispinors in Refs.^{26,27}, the width of the confining area is taken as $w + d/2$ instead of the correct value of $w + d$, leading to doubly degenerate states for $w/d = 3\ell - 1$ which differs from the tight-binding results^{35–38}. The nanoribbon limit from our nanolane model, however, provides a remarkably closer agreement with the tight-binding results. The differences appear at small widths (as our results and those of Refs.^{26,27} and the tight-binding calculations asymptotically converge at large widths). For instance, in comparison to Ref.³⁸, the results in Ref.²⁶ produce relative deviations $|\Delta\epsilon_g|/\epsilon_g$ up to around 30% (see Fig. 5 therein) when the width is reduced to $w = 4d \simeq 1$ nm. Such sizable deviations at small widths appear to be attributed to the shortcomings of the continuum model²⁶. Taking the nanoribbon limit from our model gives relative deviations of $\epsilon_g \lesssim 4\%$ in comparison with Ref.³⁸ for all w . This can be seen by noting that the energy bandgap in the limit of an arm-

chair nanoribbon from Eq. (A1) is

$$\frac{\epsilon_g}{\hbar v_F} = \frac{2\pi}{1 + w/d} \left| n + \frac{4}{3} \left(1 + \frac{w}{d} \right) \right|_{\min} \quad (\text{A2})$$

for integer n , while this quantity from the tight-binding solutions of Ref.³⁸ (appendix A therein) is

$$\frac{\epsilon_g}{\hbar v_F} = \frac{4\sqrt{3}}{3} \left| 1 + 2 \cos \left(\frac{r\pi}{N + 1} \right) \right|_{\min} \quad (\text{A3})$$

for $r = 1, 2, \dots, N$ and $N = 2(w/d) + 1$. For the thinnest gapped nanoribbon ($w = 3d$), Eqs. (A3) and (A2) give $\epsilon_g \simeq 0.54 \hbar v_F$ and $0.52 \hbar v_F$, respectively, at the relative 4% difference noted above. Our results thus indicate that the continuum modeling can remain relatively accurate down to just a couple of lattice spacings.

For the limiting case of zigzag nanoribbons, our model gives a simpler form of Eq. (A1) as $\sin[k_{\perp}(w + d)] = 0$ which produces a gapless energy band regardless of the choice of w . This agrees with the tight-binding results^{35–38}. The limiting zigzag nanoribbon obtained from our nanolane model can however be distinguished from zigzag nanoribbons in the following two aspects. First, unlike the tight-binding results, the model here gives a closed-form expression for the low-energy spectra. Second, it does not possess any edge-states. The latter is expected, as the nanolanes in our model produce no actual lattice termination edges. The edge-states also appear to signify the Dirichlet boundary conditions that are imposed asymmetrically relative to the two different honeycomb sublattices of graphene sheet in both the tight-binding^{28,38} and previous massless Dirac formulations²⁶ but not in our model.

* koohsarian.ramian@gmail.com (corresponding author)

† a.naji@ipm.ir

¹ A. K. Geim and K. S. Novoselov, Nat. Mater. 6, 183 (2007).

² A. K. Geim, Science 324, 1530 (2009).

³ K. S. Novoselov, A. K. Geim, S. V. Morozov, D. Jiang, M. I. Katsnelson, I. V. Grigorieva, S. V. Dubonos, and A. A. Firsov, Nature 438, 197 (2005).

⁴ S. Y. Zhou, G.-H. Gweon, J. Graf, A. V. Fedorov, C. D. Spataru, R. D. Diehl, Y. Kopelevich, D.-H. Lee, S. G. Louie, and A. Lanzara, Nat. Phys. 2, 595 (2006).

⁵ V. Singh, D. Joung, L. Zhai, S. Das, S.I. Khondaker, and S. Seal, Progress in materials science, 56(8), pp.1178-1271 (2011).

⁶ S.D. Sarma, S. Adam, E.H. Hwang, and E. Rossi, . Reviews of modern physics, 83(2), p.407 (2011)

⁷ A. N. Banerjee, Interface Focus 8, 20170056 (2018).

⁸ T. Zhumabek and C. Valagiannopoulos, Phys. Rev. Research 2, 043349 (2020)

⁹ D. Tulegenov and C. Valagiannopoulos, Scientific Reports 10, 13051 (2020)

¹⁰ K. S. Novoselov, A. K. Geim, S. V. Morozov, D. Jiang, M.

I. Katsnelson, I. V. Grigorieva, S. V. Dubonos, and A. A. Firsov, Nature 438, 197-200 (2005).

¹¹ A. H. Castro Neto, F. Guinea, N. M. R. Peres, K. S. Novoselov, and A. K. Geim Rev. Mod. Phys. 81, 109 (2009).

¹² D.S.L. Abergel, V. Apalkov, J. Berashevich, K. Ziegler, T. Chakraborty, Adv. Phys. 59:261-482 (2010).

¹³ K.S. Novoselov, V.I. Falko, L. Colombo, P.R. Gellert, M.G. Schwab and K. Kim, nature, 490(7419), pp.192-200 (2012).

¹⁴ C. Backes, A.M. Abdelkader, C. Alonso, A. Andrieux-Ledier, R. Arenal, J. Azpeitia, N. Balakrishnan, L. Banszerus, J. Barjon, R. Bartali and S. Bellani, 2D Materials, 7(2), p.022001 (2020).

¹⁵ S.D. Sarma, S. Adam, E.H. Hwang and E. Rossi, Reviews of modern physics, 83(2), p.407 (2011).

¹⁶ Y. Zhang, Y.W. Tan, H.L. Stormer and P. Kim, . nature, 438(7065), pp.201-204 (2005).

¹⁷ Gusynin, V.P. and Sharapov, S.G., 2005. 95(14), p.146801.

¹⁸ Bolotin, K.I., Ghahari, F., Shulman, M.D., Stormer, H.L. and Kim, P., 2009. Nature, 462(7270), pp.196-199.

¹⁹ Beenakker, C.W.J., 2008, Reviews of Modern Physics,

- 80(4), p.1337.
- ²⁰ Stander, N., Huard, B. and Goldhaber-Gordon, D., 2009. Phys. Rev. Lett. 102(2), p.026807.
 - ²¹ Jiang, X., Shi, C., Li, Z., Wang, S., Wang, Y., Yang, S., Louie, S.G. and Zhang, X., 2020. Science, 370(6523), pp.1447-1450.
 - ²² Vozmediano, M.A., Katsnelson, M.I. and Guinea, F., 2010. Physics Reports, 496(4-5), pp.109-148.
 - ²³ Miransky, V.A. and Shovkovy, I.A., 2015. Physics Reports, 576, pp.1-209.
 - ²⁴ Fialkovsky, I.V. and Vassilevich, D.V., 2012. International Journal of Modern Physics A, 27(15), p.1260007.
 - ²⁵ Fialkovsky, I.V. and Vassilevich, D.V., 2016. Modern Physics Letters A, 31(40), p.1630047.
 - ²⁶ Brey, L. and Fertig, H.A., 2006. Physical Review B, 73(23), p.235411.
 - ²⁷ Brey, L. and Fertig, H.A., 2007, Physical Review B, 75(12), p.125434.
 - ²⁸ Akhmerov A. R. and Beenakker C. W. J., 2008, Physical Review B 77, 085423
 - ²⁹ Beneventano, C.G. and Santangelo, E.M., 2012, International Journal of Modern Physics: Conference Series (Vol. 14, pp. 240-249). World Scientific Publishing Company.
 - ³⁰ Beneventano, C.G., Fialkovsky, I., Santangelo, E.M. and Vassilevich, D.V., 2014. The European Physical Journal B, 87(3), p.50.
 - ³¹ Beneventano, C.G., Fialkovsky, I., Nieto, M. and Santangelo, E.M., 2018. Physical Review B 97, 155406.
 - ³² Li, X., Wang, X., Zhang, L., Lee, S. and Dai, H., 2008. science, 319(5867), pp.1229-1232.
 - ³³ Wang, X., Ouyang, Y., Li, X., Wang, H., Guo, J. and Dai, H., 2008. Phys. Rev. Lett. 100(20), p.206803.
 - ³⁴ Schwierz, F., 2010. Nature nanotechnology, 5(7), p.487.
 - ³⁵ Nakada, K., M. Fujita, G. Dresselhaus, and M. S. Dresselhaus, 1996, Phys. Rev. B 54, 17954
 - ³⁶ Fujita, M., Wakabayashi, K., Nakada, K. and Kusakabe, K., 1996. Journal of the Physical Society of Japan, 65(7), pp.1920-1923.
 - ³⁷ Ezawa, M., 2006. Physical Review B, 73(4), p.045432.
 - ³⁸ Wakabayashi, K., Sasaki, K.I., Nakanishi, T. and Enoki, T., 2010. Sci. Technol. Adv. Mater. 11, 054504
 - ³⁹ Son, Y.W., Cohen, M.L. and Louie, S.G., 2006. Phys. Rev. Lett. 97(21), p.216803.
 - ⁴⁰ Yang, L., Park, C.H., Son, Y.W., Cohen, M.L. and Louie, S.G., 2007. Physical Review Letters, 99(18), p.186801.
 - ⁴¹ Barone, V., Hod, O. and Scuseria, G.E., 2006. Nano letters, 6(12), pp.2748-2754.
 - ⁴² A. Chodos, R.L. Jaffe, K. Johnson, C.B. Thorn, V.F. Weisskopf, Phys. Rev. D 9, 3471-3495 (1974).
 - ⁴³ A. Chodos, R.L. Jaffe, K. Johnson, and C.B. Thorn, Phys. Rev. D 10, 2599 (1974).
 - ⁴⁴ T.A. DeGrand, R.L. Jaffe, K. Johnson, and J. Kiskis, Phys. Rev. D L2, 2060 (1975).
 - ⁴⁵ K. Johnson, Acta Phys. Polonica B 6, 865 (1975).
 - ⁴⁶ P. Hasenfratz and J. Kuti, Phys. Rep. **40**, 75 (1978).
 - ⁴⁷ A. W. Thomas and W. Weise, *The Structure of the Nucleon* (Wiley-VCH, Berlin, 2001).
 - ⁴⁸ K.T. Hecht, *Quantum Mechanics* (Springer, New York, 2000).
 - ⁴⁹ M. Berry and R. J. Mondragon, Proc. R. Soc. London A 412, 53 (1987).
 - ⁵⁰ Li, X., Wang, X., Zhang, L., Lee, S. and Dai, H., 2008. science, 319(5867), pp.1229-1232.
 - ⁵¹ Chen, Z., Narita, A. and Müllen, K., 2020. 32(45), p.2001893.
 - ⁵² Han, M.Y., Özyilmaz, B., Zhang, Y. and Kim, P., 2007. Phys. Rev. Lett. 98(20), p.206805.
 - ⁵³ Liu, C., Zhang, J., Muruganathan, M., Mizuta, H., Oshima, Y. and Zhang, X., 2020. Carbon, 165, pp.476-483.
 - ⁵⁴ Kimouche, A., Ervasti, M.M., Drost, R., Halonen, S., Harju, A., Joensuu, P.M., Sainio, J. and Liljeroth, P., 2015. Nature communications, 6(1), pp.1-6.